ACI MATERIALS JOURNAL TECHNICAL PAPER

Title no. 87-M68

# Dependence of Flexural Behavior of Fiber Reinforced Mortar on Material Fracture Resistance and Beam Size

by Robert J. Ward and Victor C. Li

*The flexural load-deflection curves for mortar reinforced with various fiber types (steel and synthetic) and various fiber volume fractions are measured using three different beam sizes. Three new flexural toughness indexes that reflect the general shape of the load-deflection curve are defined and calculated. The flexural strength/tensile strength ratio $f_f/f_t'$ is proposed as a parameter that reflects material brittleness — a lower value for a more brittle material. Good correlations between two of the new flexural toughness indexes and parameters that involve only $f_f$, $f_t$ and the fiber length are found. These results indicate the possibility of getting a good idea of the flexural load-deflection curve by measuring only $f_f$ and $f_t$ in the laboratory. By realizing the dependence of structural behavior on material fracture resistance, and also the ability of the parameters $f_f$ and $f_t$ to characterize this dependence, it is possible to develop simple formulas that directly express this dependence.*

**Keywords: beams (supports);** compressive strength; fiber reinforced concretes; **flexural strength;** fracture properties; load-deflection curve; **metal fibers; mortars (material); reinforcing materials;** shear strength; splitting tensile strength; **synthetic fibers.**

Conventional concrete design has relied almost exclusively on compressive strength as a means of specifying the concrete quality. Other concrete properties, such as tensile strength, modulus, durability, etc., have been empirically related to the compressive strength. However, the recent development and ever-increasing use of both high-strength concrete (130 MPa compressive strength concrete was used in Seattle's Two Union Square Building) and fiber reinforced concrete has forced us to look more closely at concrete properties other than the compressive strength. Ordinary strength concrete fails by aggregates pulling out of the matrix, resulting in a rough fracture surface. In contrast, high-strength concrete, because of the high interfacial-bond strength between the aggregate and the mortar, fails by cracks passing straight through the aggregate, resulting in a smooth fracture plane. Concrete reinforced with low-volume fractions (up to 2 percent) of short fibers has a compressive strength very similar to that of the unreinforced concrete, but exhibits much greater resistance to crack formation and growth. It is obvious that compressive strength alone is not adequate for the design of fiber concrete structures.

Material fracture resistance is an important property that can successfully distinguish between the failure modes of high-strength concrete, ordinary strength concrete, and fiber reinforced concrete. The complete tensile behavior of concrete can be defined using the stress-strain curve and the tension-softening curve. Hillerborg[1] introduced the material characteristic length $l_{ch} = G_F E/f_t^2$ to define material tensile brittleness. $G_F$ is the fracture energy, $E$ is the Young's modulus, and $f_t$ is the tensile strength. $l_{ch}$ is a measure of the ratio of the upward slope of the stress-strain curve to the downward slope of the tension-softening curve. A material with a relatively sharp descending softening curve has a low $l_{ch}$ value and is perceived as being relatively brittle. Since high-strength concrete attains a relatively high tensile strength and then cracks along a smooth fracture plane without aggregate pullout, it has been shown that its softening curve has a relatively sharp descent compared to plain concrete, and thus the material is more brittle, with a lower $l_{ch}$. Fiber reinforced concrete, on the other hand, has been shown to have a relatively flat softening curve compared to the plain concrete, and is thus more ductile, with higher $l_{ch}$. Hillerborg[2] presented the results of theoretical analyses performed by Petersson[3] and Gustafsson,[4] which showed the ratios $f_f/f_t$ and $f_v/f_t$, respectively, as increasing functions of the parameter $l_{ch}/d$, where $f_f$ is the flexural strength of an unreinforced beam, $f_v$ is the shear strength of a longitudinally reinforced beam, and $d$ is the beam depth. $l_{ch}/d$ is a structural brittleness parameter, with more brittle behavior being observed when the material characteristic length decreases or the structural size in-

*ACI Materials Journal*, v. 87, No. 6, November-December 1990.
Received May 8, 1989, and reviewed under Institute publication policies.

*Victor C. Li, Associate Professor of Civil Engineering at the University of Michigan at Ann Arbor, is a specialist in the fracture mechanics of quasibrittle materials. Dr. Li's principal research interests are micro/meso-mechanics, experimental testing, and materials engineering of cement and ceramic composites. He has more than 30 publications in the field and has served on a number of international scientific advisory boards.*

*Robert J. Ward holds an MS degree in civil engineering from the Massachusetts Institute of Technology. He is presently a structural engineer with Cygna Consulting Engineers in Boston, Massachusetts.*

creases. These analyses show the dependence of structural strengths $f_f$ and $f_v$ on the material tensile fracture properties $f_t$ and $l_{ch}$. However, the tension-softening curve is, in general, too difficult and too time-consuming to measure for practical implementation in routine design and quality control.

Researchers have attempted to use the flexural load-deflection curve rather than the softening curve as a means of quantifying the improved fracture resistance of fiber concrete. The advantage of this procedure is that the test is relatively simple to perform and closely simulates many of the loading conditions imposed on fiber concrete in practical applications. However, the disadvantages of this method are that the curve depends on the specimen size and geometry, and the loading configuration. It is also more difficult to use a complete curve rather than just a single parameter (such as $G_F$ or $l_{ch}$) in design. Numerous researchers have proposed using flexural-toughness indexes, which are defined using the flexural load-deflection curve as a means of getting around these problems. Henager[5] proposed indexes based on the point of first crack on the load-deflection curve. Johnston[6] proposed indexes $I_5$, $I_{10}$, and $I_{30}$ based on the area under the curve up to certain defined deflection values. Wang and Backer[7] described new indexes that are more sensitive to the post-peak shape of the load-deflection curve. The disadvantages of the previously mentioned indexes are that it is difficult to locate accurately the position of first crack on the load-deflection curve, relatively time-consuming to record a complete load-deflection curve (compared, for example, to measuring only the compressive strength), and difficult to use a set of indexes for the purposes of design and quality control. The flexural load-deflection curve can, however, tell us a great deal about material fracture resistance properties.

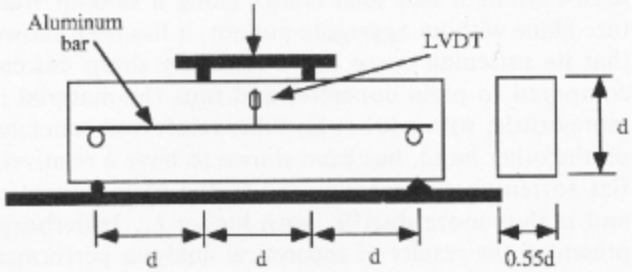


*Fig. 1 — Specimen geometry and loading configuration for flexural test*

**Table 1 — Fiber properties**

| Fiber type | Length, mm | Aspect ratio $1/d_{eq}$ | Tensile strength, MPa | Modulus, GPa | Density, g/cc | Surface |
|---|---|---|---|---|---|---|
| Steel | 25.0 | 28.5 | 1000 | 200 | 7.9 | Crimped |
| Steel | 50.0 | 57 | 1000 | 200 | 7.9 | Crimped |
| Aramid | 6.4 | 530 | 2800 | 130 | 1.45 | Straight |
| Acrylic | 6.4 | 470 | 400 | 6 | 1.15 | Straight |
| High-modulus polyethylene | 12.7 | 334 | 2000 | 100 | 0.97 | Straight |

1 mm = 0.0394 in.; 1 g/cc = 0.0361 lb/in.$^3$; 1 MPa = 145 psi.

## RESEARCH SIGNIFICANCE

The aim of this research is to examine how changes in material brittleness can lead to changes in structural behavior, particularly flexural performance. Material brittleness is varied by reinforcing plain mortar with various fiber types (steel and synthetic) and by using various volume fractions. The possibility of characterizing the tensile fracture properties of a nonyielding material like concrete, using only the flexural and first crack splitting tensile strengths, is successfully demonstrated. This is a simple procedure, ideally suited for design purposes, and should encourage engineers to make greater use of both fiber reinforced concrete and high-strength concrete in future practical applications. These research findings can be used to devise a future program of testing on practical plain concrete and fiber reinforced concrete mixes, the results of which could be used in design codes so that material brittleness may be better accounted for.

## EXPERIMENTAL PROGRAM

Four different beam sizes, all with similar geometries, were tested under third-point bending, as shown in Fig. 1, to examine the influence of beam size on the flexural strength and flexural load-deflection curve. Plain mortar, as well as mortar reinforced with various volume fractions of steel, aramid, high-modulus polyethylene, and acrylic fibers, were used in the beams to investigate the effects of material fracture resistance on the flexural behavior. The fiber properties are listed in Table 1. A total of 129 beams (in sets of three nominally identical specimens) were tested to give results for 43 different combinations of beam size, fiber type, and fiber volume fraction. The beam depths used were 63.5, 114, 171, and 228 mm (2.5, 4.5, 6.75, and 9 in.). A constant mortar mix with a cement:sand:water ratio of 1:1:0.4 by weight was used. The cement was Type III rapid hardening and the sand passed through a #8 sieve. Volume fractions of 0.5, 1.0, 1.5, and 2.0 percent were used with the 25 mm (1 in.) steel fibers; 1.0 and 2.0 percent with the 50 mm (2 in.) steel fibers; 0.5, 1.0, and 1.5 percent with the aramid fibers; 1.0 and 2.0 percent with the acrylic fibers; and 1.0 percent with the high-modulus polyethylene fibers. All the materials were added initially to a bladeless mixer and mixing was performed for about 3 min. Superplasticizer was used with the synthetic fibers to insure adequate workability. All beams were tested perpendicular to the casting direction. The specimens were covered with plastic after casting for about 12 to 14 hr and were then demolded and stored in air at 20 C (68 F) until testing at between

**Table 2 — Flexural, splitting tensile, and compressive strengths of various fiber reinforced mortar**

| Fiber type | Length, mm | $V_f$, percent | Flexural strength, $d$ = 63.5, MPa | $d$ = 114, MPa | $d$ = 171, MPa | $d$ = 228, MPa | Splitting tensile strength, Crack, MPa | Maximum, MPa | Compressive strength, MPa |
|---|---|---|---|---|---|---|---|---|---|
| Plain mortar | | 0 | 3.0 | 2.6 | 2.3 | 2.4 | 2.9 | 2.9 | 57.0 |
| Aramid | 6.4 | 0.5 | 4.9 | 4.1 | 4.0 | 3.9 | 4.2 | 4.2 | 52.1 |
| Aramid | 6.4 | 1.0 | 5.5 | 5.1 | 4.7 | 5.1 | 4.4 | 4.4 | 50.3 |
| Aramid | 6.4 | 1.5 | 6.9 | 6.1 | 6.0 | 5.5 | 4.6 | 4.6 | 45.5 |
| Steel | 25 | 0.5 | 3.6 | 3.5 | 3.5 | 3.5 | 3.6 | 5.6 | 58.9 |
| Steel | 25 | 1.0 | 5.1 | 5.4 | 4.9 | 4.7 | 3.9 | 6.0 | 62.6 |
| Steel | 25 | 1.5 | 6.4 | 6.2 | 5.7 | 5.5 | 4.8 | 5.9 | 59.7 |
| Steel | 25 | 2.0 | 7.0 | 7.0 | 6.6 | 6.6 | 4.8 | 5.6 | 57.0 |
| Steel | 50 | 1.0 | | 7.4 | | 6.2 | 4.3 | 6.2 | 54.1 |
| Steel | 50 | 2.0 | | 8.9 | | 7.8 | 5.6 | 7.6 | |
| Acrylic | 6.4 | 1.0 | | 4.0 | | 3.4 | 4.3 | 4.3 | 45.3 |
| Acrylic | 6.4 | 2.0 | | 3.7 | | 3.5 | 3.6 | 3.6 | 33.0 |
| High-modulus polyethylene | 12.7 | 1.0 | | 8.9 | | 7.7 | 3.2 | 6.4 | 45.7 |

Beam depth in mm: 1 mm = 0.0394 in.; 1 MPa = 145 psi.

14 and 16 days of age. Complete details of the testing program are given by Ward.[5]

Testing was carried out in a displacement-controlled testing machine. All beams of a similar size were loaded with similar initial cross-head speeds and the actual speed was changed in proportion to the beam depth. The initial speed for the 114 mm (4.5 in.) beams was 0.6 mm/min (0.024 in./min). Sometime after the maximum load was reached, the loading rate was increased to insure a reasonable testing time. The load was applied to the top of the beam through two rectangular cross section loading platens placed across the full width of the beam. The width of these platens was 0.11 times the beam depth. A linear variable differential transformer (LVDT) was placed at the center of each of the three larger sized beams to measure the midspan deflection. All tests were continued until the load dropped below 10 percent of the maximum value. All the plain mortar beams failed suddenly at the maximum load, and so it was not possible to measure the descending branch of the flexural load-deflection curve.

A total of 91 cylinders [77 mm (3 in.) diameter x 154 mm (6 in.) long] were also tested to give average values for the compressive strength (average of three tests) and

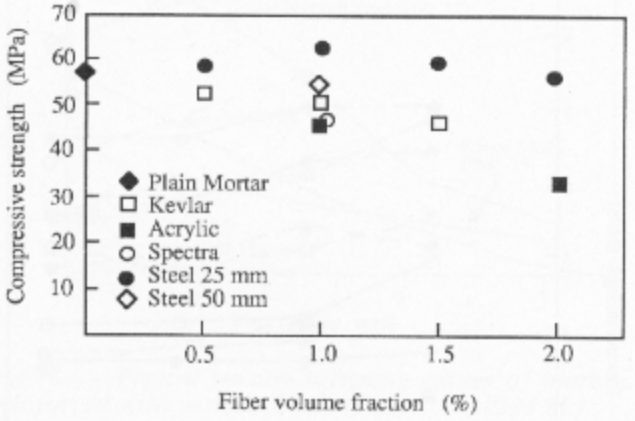


*Fig. 2 — Effect of fiber reinforcement on compressive strength (1 mm = 0.0394 in.; 1 MPa = 145 psi)*

kg/m³; and coarse aggregate [5 to 20 mm (0.2 to 0.8 in.)] (823, 329, 1141, and 1711 lb/yd³, respectively).

The cement:sand:water ratio for this mix is 1:1.39:0.4, compared to a ratio of 1:1:0.4 used in the test program. The volume fraction of coarse aggregate in the mix would be about 40 percent (assuming a coarse aggregate relative density of 2.6). If a 1 percent

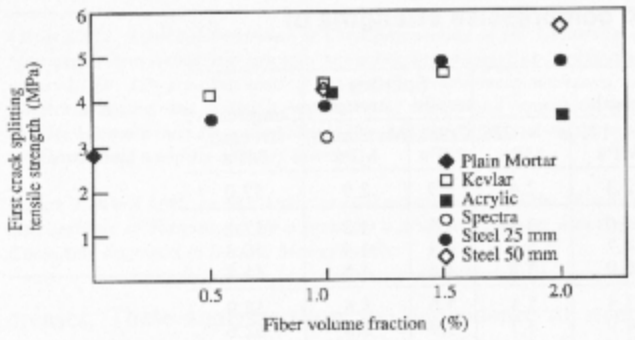


*Fig. 3 — Effect of fiber reinforcement on the first crack splitting tensile strength (1 mm = 0.0394 in.; 1 MPa = 145 psi)*

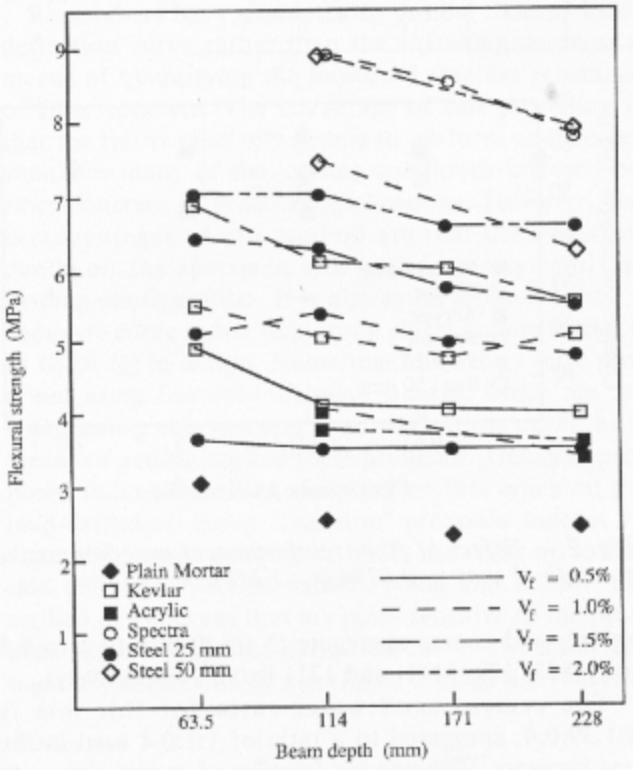


*Fig. 4 — Influence of beam size on flexural strength (1 mm = 0.0394 in.; 1 MPa = 145 psi)*

creases of the order of 20 percent were noted at a volume fraction of 1 percent. These strength reductions may be related to porosity increases due to compaction difficulties with high aspect ratio flexible fibers.

## Splitting tensile strength

The first crack and maximum splitting tensile strengths are listed in Table 2. Fig. 3 illustrates the effects of fiber type and volume fraction on the first crack strength. This strength was calculated from the load at which the first visible crack appeared across the cylinder. In many cases, the appearance of the crack was accompanied by a low popping sound. In general, the cracking tensile strength increases with fiber volume fraction. Aramid fibers give much higher cracking strength than high-modulus polyethylene, probably because of their higher bond strength with mortar. Due to their relatively good bond strength and high aspect ratio, the 6.4 mm (0.25 in.) aramid fibers can provide similar cracking strengths to those provided by the 25 mm (1 in.) steel fibers. A 2 percent volume fraction of acrylic fibers provides a low tensile strength, mainly because of compaction problems with resulting high porosity. The maximum loads recorded in the splitting test are not considered meaningful because of unknown stress distribution after cracking. It is interesting, however, that for the plain mortar and acrylic and aramid fiber mortar specimens, the first crack and maximum loads correspond, whereas there are substantial differences (up to 100 percent) for the high-modulus polyethylene and steel fiber mortars, due to the greater ability of these fibers to transfer relatively high stresses after composite cracking.

## Flexural strength

The flexural strengths for each material and each beam size (corrected for the effects of loading fixtures and beam self-weight) are listed in Table 2. Fig. 4 illustrates similar trends of decreasing strength as beam size increases for all the materials. Other investigators related strength reductions to the volume of material within a probable failure zone. For beams with similar geometries, the material volume is a function of the beam depth and, for these cases, Johnston[9] found the strength of plain concrete and steel fiber concrete beams approximately proportional to $d^{-0.3}$; Akihama, Suenaga, and Nakagawa[10] found the strength of carbon fiber reinforced concrete beams approximately proportional to $d^{-0.374}$; and Torrent and Brooks[11] found the strength of plain concrete beams approximately proportional to $d^{-0.123}$. The flexural strength values shown in Fig. 4 decrease, on average, in proportion to $d^{-0.13}$. Far less dependence on material volume is exhibited than that proposed by Johnston or Akihama. The reasons for this may lie with the loading fixtures, material type, curing process, or effects of beam self-weight. Petersson's analytical results,[3] showing decreasing $f_f/f_t$ ratios as the parameter $d/l_{ch}$ increased, are summarized in Fig. 5. These results are based on a fracture mechanics approach: the size dependence of structural strength stems from the fact that elastic energy is stored and released throughout the beam at a rate proportional to the beam volume (for similar geometries), whereas the energy absorption rate across the critical fracture plane only increases in proportion to the beam cross section size. These results are not exactly applicable to concrete because they are based on an assumed linear elastic stress-strain curve, whereas the true curve shows significant nonlinearity and inelastic deformations. Assuming a Weibull distribution for concrete strength also leads to a structural size effect because of a greater chance of a weaker section in a larger specimen. To fully understand the size dependence of structural strength, it is necessary to consider energy absorption and release rates in conjunction with the Weibull

strength distribution. Ward[8] gives a short discussion of this approach and shows some typical results.

The theoretical results from Petersson[3] presented in Fig. 5 suggest that the flexural strength depends on both the tensile strength and the material characteristic length. Fig. 6 illustrates representations of typical tension-softening curves for the materials used in this program. The plain mortar and synthetic fiber mortar curves were measured in earlier testing programs,[12,13] using mortar with a cement:sand:water ratio of 1:1:0.5 and the same fibers used in this testing program. The steel fiber mortar curves are taken from results presented by Hillerborg.[14] It may be expected that the 25 mm (1 in.) steel fibers used in this testing program have similar shaped $\sigma - \delta$ curves to that shown for the round steel fibers, and the 50 mm (2 in.) fibers have similar shaped curves to that shown for the indented steel fibers. Hillerborg[14] defined an effective $G_F'$ and $l_{ch}'$, based on a continuation of the initial slope of the softening curve as a straight line down to meet $\sigma = 0$, and he suggested that the $f_f/f_t$ ratio was related to $l_{ch}'$. He considered the area under the softening curve at large crack openings to have little influence on the maximum beam strength. If an effective $l_{ch}'$ was calculated, based on the softening curves in Fig. 6, the plain mortar would have the lowest value, the acrylic fiber mortar would be next lowest, the aramid and 25 mm (1 in.) steel fiber mortars would give the next lowest values, and the 50 mm (2 in.) steel and high-modulus polyethylene fiber mortars would have the highest values. The effective characteristic length would increase as fiber volume fraction increased and the material became less brittle. Fig. 7 shows the $f_f/f_t$ ratios for each fiber type and volume fraction, calculated using the flexural strengths of the 114 mm (4.5 in.) beams. Direct correlation between the trend of increasing $f_f/f_t$ ratios and increasing material characteristic lengths just mentioned can be seen. This confirms the dependence of flexural strength on material brittleness, as well as on tensile strength.

The very high $f_f/f_t$ ratio of the high-modulus polyethylene fiber mortar may be explained as follows. Due to the relatively low tensile cracking strength of this material, a flexural crack formed at the bottom of the beam at a relatively small load in the flexural test. However, because of the relatively flat initial slope of the softening curve, with perhaps some initial stress increase as the fibers are stretched after the composite cracks, the load continued to increase after the flexural cracks developed. Subsequently, a number of cracks formed in the high-moment central span zone. On a macroscopic scale, the behavior was almost like the yielding of steel once the elastic bending moment capacity is passed. This multiple cracking allowed deformations to exist within the beam that were compatible with developing relatively high tensile stresses over a large proportion of the beam depth. The theoretical limit of the $f_f/f_t$ ratio is 3.0 if the tensile strength is developed over the full beam depth, and an infinitesimal compression zone exists at the top of the beam. The

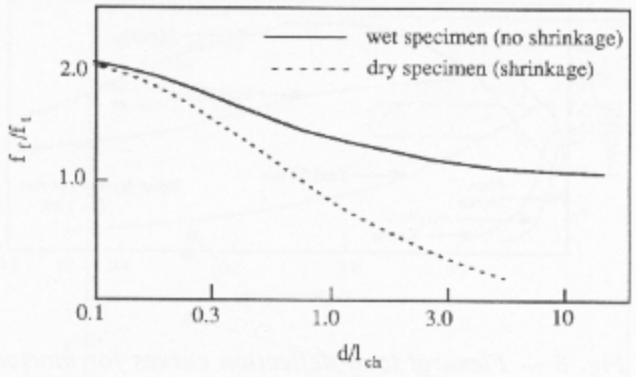


*Fig. 5 — Theoretical curves relating the $f_f/f_t$ ratio to the $d/l_{ch}$ ratio calculated using the fictitious crack model*

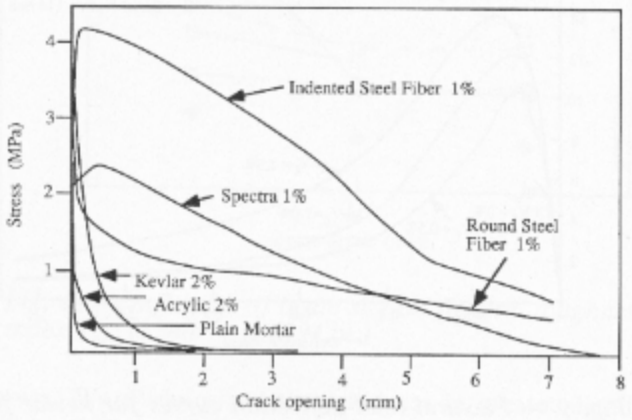


*Fig. 6 — Typical tension-softening curves of mortars reinforced with various fibers (1 mm = 0.0394 in.)*

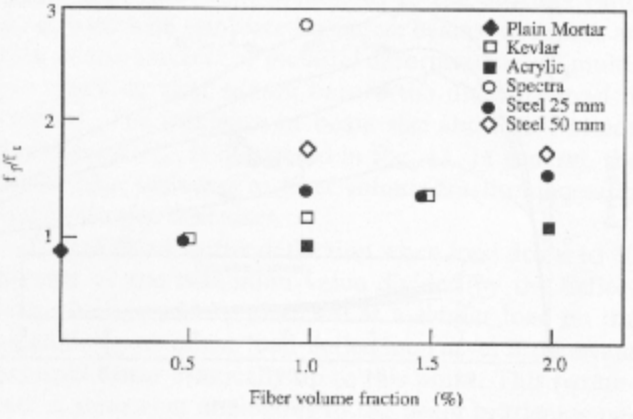


*Fig. 7 — Effect of fiber reinforcement on the ratio between flexural and splitting tensile strengths (1 mm = 0.0394 in.)*

$f_f/f_t$ ratio of the 114 mm (4.5 in.) high-modulus polyethylene fiber beams is 2.78.

## Flexural load-deflection curves

Fig. 8 shows typical flexural load-deflection curves for each fiber type. Due to inadequate machine stiffness, it was not possible to measure the descending branch of the plain mortar curve. The aramid and acrylic fiber mortars show relatively sharp drops from the peak load. This is due to the relative shortness of these fibers and also to the fact that these fibers tend to

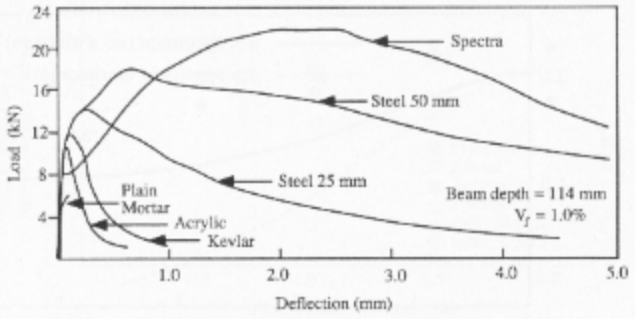


*Fig. 8 — Flexural load-deflection curves for mortars reinforced with various fiber types (1 mm = 0.0394 in.; 1 kN = 224.8 lbs)*

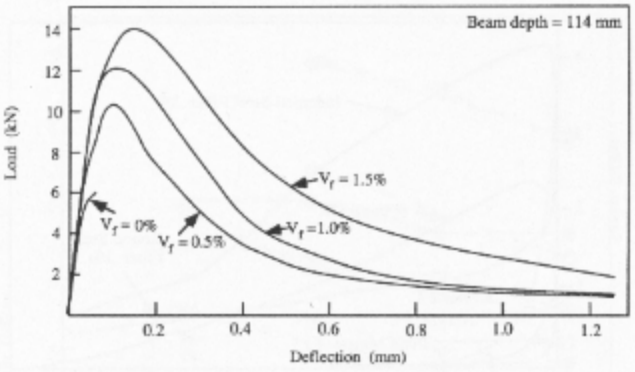


*Fig. 9 — Flexural load-deflection curves for kevlar fiber reinforced mortar beams (1 mm = 0.0394 in.; 1 kN = 224.8 lbs)*

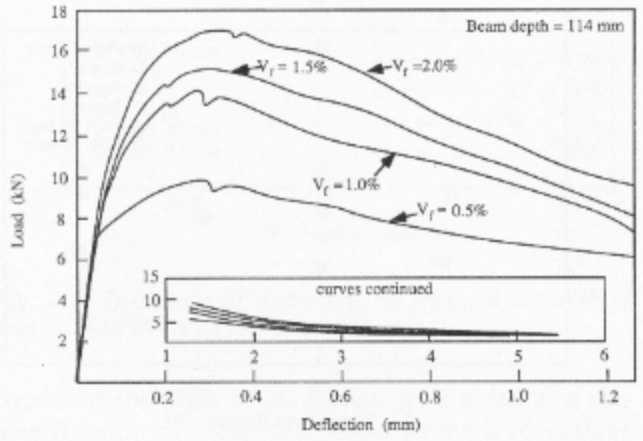


*Fig. 10 — Flexural load-deflection curves for steel fiber (25 mm) reinforced mortar beams (1 mm = 0.0394 in.; 1 kN = 224.8 lbs)*

form rod-like bundles in the matrix around which the crack propagates, thus giving a higher tensile strength but not giving much fiber pullout. The longer steel fibers show a much more gradual fall-off in load capacity as they pull out of the matrix. The very large deflection in the high-modulus polyethylene fiber mortar beam at the maximum load is due to widespread multiple cracking. The initial correspondence of all the curves is consistent with the generally held view that low-volume fractions of short fiber reinforcement do

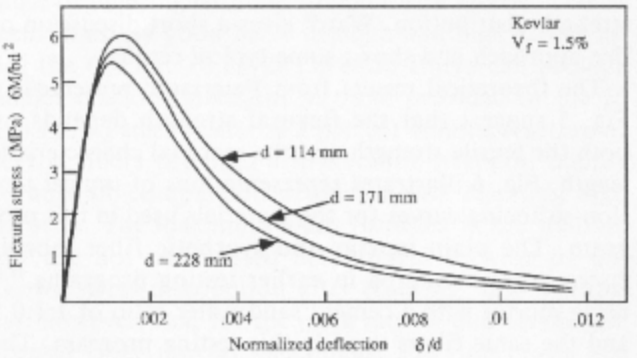


*Fig. 11 — Flexural stress versus normalized deflection for different beam sizes of kevlar fiber reinforced mortar (1 mm = 0.0394 in.; 1 MPa = 145 psi)*

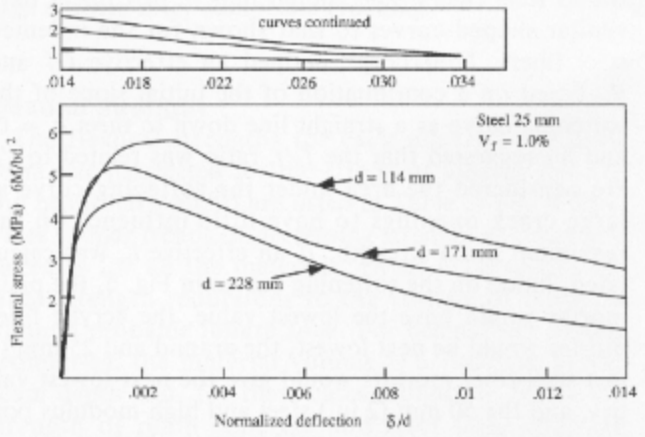


*Fig. 12 — Flexural stress versus normalized deflection for different beam sizes of steel fiber reinforced mortar (1 mm = 0.0394 in.; 1 MPa = 145 psi)*

not significantly change the composite behavior prior to matrix microcracking.[15,16]

Fig. 9 and 10 show the effects of fiber volume fraction on the flexural load-deflection curves for the aramid and 25 mm (1 in.) steel fibers. The initial linear elastic part of the curves before matrix microcracking does not change with fiber volume fraction. Energy-absorption capacity increases with fiber-volume fraction. This is because of an increase in the inelastic energy absorbed throughout the beam and also because of the fracture energy absorbed across the critical fracture plane. The higher tensile strength insures larger stresses and strains and the higher flexural strength insures more material being stressed beyond the elastic limit. The increase in fracture energy stems from a greater number of fibers bridging the crack and a more tortuous crack propagation path as the volume fraction increases.

Fig. 11 and 12 illustrate the influence of beam size on the normalized load versus normalized deflection curves for the aramid and 25 mm (1 in.) steel fibers. The normalized load is a measure of the flexural stresses in the beam and is defined as $6M/bd^2$ where $M$ is the bending moment along the beam central span and $b$ is the beam width. The normalized deflection corresponds to the midspan deflection divided by the beam depth, and is a

measure of the average strains in the beam. These curves are somewhat analogous to the stress versus normalized displacement (average strain) curves obtained from a direct tension test. In the direct tension test, the material initially strains uniformly throughout its length. At the maximum load, a localized fracture zone develops with subsequent increases in deformation within this zone, and decreases in deformation due to elastic rebound outside this zone.[17] The shape of the descending curve is thus dependent on the relative magnitude of these two deformation changes which, in turn, depends on specimen length, i.e., a longer specimen producing a sharper drop in the curve after maximum load. Increasing the beam size in a flexural test has a somewhat similar influence on the stress-normalized deflection curve.

The total area under the load-deflection curve is indicative of the energy absorbed by the beam. The coincidence of the initial linear elastic parts of the stress-normalized deflection curves in Fig. 11 and 12 confirms that the rate of elastic energy absorption is proportional to beam volume, for similar geometries. After matrix microcracking initiates, inelastic energy is absorbed throughout the more highly stressed parts of the beam, at a rate proportional to the beam volume. However, energy absorbed by the critical fracture zone is proportional to the beam cross-sectional size, and this partly accounts for the size dependence of the normalized load-deflection curves. A second contribution to the size-effect can be attributed to the reduced flexural strength as beam size increases, resulting in less material (proportionally) being stressed beyond its elastic limit and, thus, less inelastic energy being absorbed per unit volume of beam. It is possible to qualitatively express the energy-absorption capacity of a beam in flexure by

$$U = k_1 bd^2 + G_F bd \quad (1)$$

where $k_1$ accounts for energy absorbed per unit beam volume away from the critical fracture zone. The factor $k_1$ may be expected to be a decreasing function of beam size. Normalization of Eq. (1) leads to

$$U/bd^2 = k_1 + G_F/d \quad (2)$$

which illustrates normalized energy absorption as a decreasing function of beam size.

## Flexural toughness indexes

The $I_5$, $I_{10}$, and $I_{30}$ indexes defined by Johnston were calculated for each material and beam size. A full description of these calculations and results is given by Ward.[8] Table 3 lists the calculated values. A complete set of indexes can give a good idea of the general shape of the load-deflection curve. However, these indexes do not efficiently provide a characterization of material behavior or the flexural load curve.

Three new flexural toughness indexes are now defined which effectively characterize flexural performance. Ward[8] described these indexes in greater detail. Table 3 lists each index value for all the materials and each beam size. $T_{max}$ is defined as the beam deflection at maximum load divided by the deflection, at first crack. It is somewhat analogous to the ductility ratio $\phi_u/\phi_y$ used with reinforced concrete beams, and gives an idea of the amount of inelastic deformation and multiple cracking that occurs before the ultimate load is reached. The influence of beam size and fiber-volume fraction on $T_{max}$ is illustrated in Fig. 13. In general, the index value increases as fiber volume fraction increases and beam size decreases.

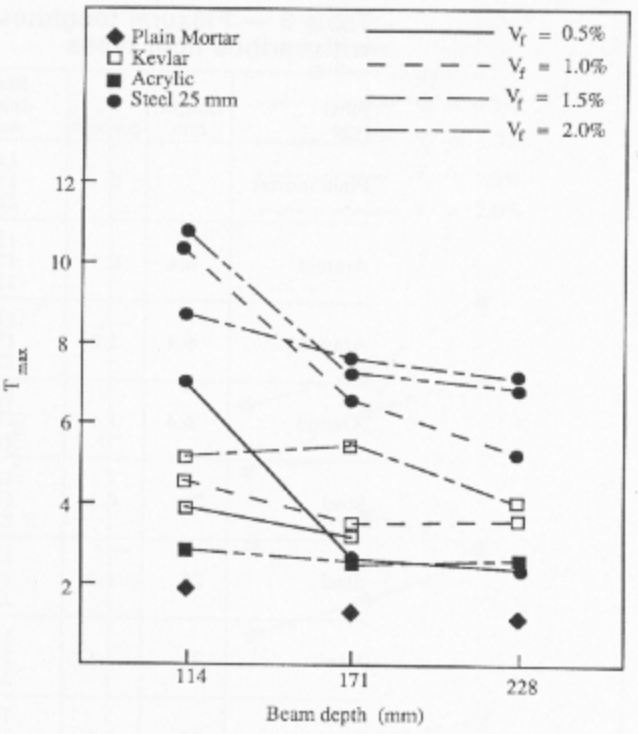


*Fig. 13 — Influence of beam size on flexural toughness index $T_{max}$ (1 mm = 0.0394 in.)*

$T_{50}$ is defined as the deflection when load drops to 50 percent of the maximum value divided by the deflection which would be observed at a similar load on the ascending part of the load-deflection curve, if the beam behaved linear elastically up to this point. This parameter is somewhat analogous to the beam brittleness parameter $l_{ch}/d$ used by Hillerborg. It reflects a beam's ability to absorb energy by inelastic deformation relative to the rate at which it stores or releases elastic energy. Fig. 14 illustrates the influence of beam size and fiber-volume fraction on $T_{50}$. For a given fiber type, the fiber-volume fraction does not significantly influence $T_{50}$. This is because flexural strength and energy capacity increase in similar proportions. It is interesting to compare this behavior with that of plain concrete when it is changed from ordinary strength to high-strength. The proportional increase in strength is greater than the proportional increase in energy capacity, leading to more brittle behavior.

$T_{10}$ is defined as the total area under the load-deflection curve up to the point where the load drops to 10

**Table 3 — Flexural toughness indexes of mortars reinforced with various fiber types**

| Fiber type | Length, mm | $V_f$, percent | Beam depth, mm | $I_5$ | $I_{10}$ | $I_{30}$ | $I_{50}$ | $T_{max}$ | $T_{50}$ | $T_{50}$, kN/m |
|---|---|---|---|---|---|---|---|---|---|---|
| Plain mortar | | 0 | 114 | | | | | 1.8 | | |
| | | | 171 | | | | | 1.3 | | |
| | | | 228 | | | | | 1.2 | | |
| Aramid | 6.4 | 0.5 | 114 | 6.9 | 14.9 | 33.9 | 42.0 | 3.9 | 13.6 | 0.53 |
| | | | 171 | 6.9 | 14.8 | 31.3 | 37.4 | 3.1 | 11.1 | 0.70 |
| | | | 228 | 6.7 | 12.9 | 21.9 | 24.2 | 2.5 | 8.0 | 0.53 |
| Aramid | 6.4 | 1.0 | 114 | 7.8 | 17.7 | 41.3 | 49.2 | 4.5 | 11.1 | 0.61 |
| | | | 171 | 7.4 | 16.7 | 35.2 | 41.2 | 3.4 | 10.0 | 0.76 |
| | | | 228 | 7.7 | 17.2 | 33.9 | 37.6 | 3.5 | 9.0 | 0.89 |
| Aramid | 6.4 | 1.5 | 114 | 7.9 | 19.4 | 55.0 | 70.8 | 5.1 | 12.9 | 1.00 |
| | | | 171 | 7.7 | 19.6 | 54.6 | 67.8 | 5.4 | 10.7 | 1.34 |
| | | | 228 | 7.8 | 18.7 | 46.1 | 54.0 | 3.9 | 11.0 | 1.48 |
| Steel | 25 | 0.5 | 114 | 6.5 | 12.0 | 36.4 | 58.8 | 7.0 | 66.5 | 2.26 |
| | | | 171 | 6.8 | 12.2 | 34.7 | 52.8 | 2.6 | 42.0 | 2.57 |
| | | | 228 | 6.6 | 13.0 | 36.0 | 53.2 | 2.4 | 40.5 | 2.91 |
| Steel | 25 | 1.0 | 114 | 7.5 | 17.2 | 55.3 | 88.8 | 10.4 | 40.5 | 3.05 |
| | | | 171 | 7.1 | 17.9 | 48.5 | 83.1 | 6.5 | 31.3 | 3.32 |
| | | | 228 | 7.4 | 16.0 | 46.8 | 69.9 | 5.2 | 28.2 | 3.00 |
| Steel | 25 | 1.5 | 114 | 8.0 | 19.9 | 75.2 | 116.0 | 8.7 | 37.0 | 3.70 |
| | | | 171 | 8.1 | 20.4 | 70.7 | 111.7 | 7.5 | 31.0 | 4.20 |
| | | | 228 | 7.5 | 18.1 | 59.4 | 92.4 | 7.0 | 30.0 | 4.50 |
| Steel | 25 | 2.0 | 114 | 7.8 | 19.0 | 79.8 | 122.2 | 10.7 | 35.0 | 4.26 |
| | | | 171 | 7.9 | 19.6 | 68.6 | 109.0 | 7.2 | 32.2 | 4.35 |
| | | | 228 | 8.0 | 20.7 | 68.0 | 91.3 | 6.9 | 24.4 | 5.03 |
| Steel | 50 | 1.0 | 114 | 6.4 | 15.4 | 64.5 | 123.0 | 22.6 | 106.1 | 13.90 |
| Steel | 50 | 2.0 | 114 | 6.9 | 17.3 | 75.7 | 146.0 | 22.3 | 99.2 | 18.20 |
| Acrylic | 6.4 | 1.0 | 114 | 6.9 | 13.0 | 21.4 | | 2.5 | 8.0 | 0.26 |
| | | | 228 | | | | | 1.8 | | |
| Acrylic | 6.4 | 2.0 | 114 | 6.4 | 12.2 | 25.3 | | 2.8 | 12.0 | 0.36 |
| | | | 228 | 5.9 | 9.9 | 13.6 | | 2.5 | 6.4 | 0.36 |
| High-modulus polyethylene | 12.7 | 1.0 | 114 | 6.2 | 13.0 | 50.2 | 94.7 | 66.6 | 97.0 | 16.60 |

1 mm = 0.0394 in.; 1 kN/m = 5.7 lb/in.

percent of the maximum value, divided by the beam cross-sectional area. It correlates approximately with the total energy-absorption capacity of the beam. If inelastic energy absorption outside the fracture zone is small, then it correlates with the fracture energy. Fig. 15 illustrates the influence of beam size and fiber-volume fraction on $T_{10}$. As beam size increases, so does the ratio between distributed inelastic energy absorbed (proportional to beam volume) and energy absorbed (proportional to beam section size), and this more than compensates for energy-absorption losses due to lower flexural strengths, resulting in increasing $T_{10}$ values as beam size increases. The $T_{10}$ value also reflects the increases in energy-absorption capacity as the fiber-volume fraction is increased.

## SIMPLE ESTIMATES OF FLEXURAL TOUGHNESS

The ability of the flexural load-deflection curve to distinguish the behavior of mortar reinforced with various fiber types and volume fractions has been demonstrated. Also, the ability of flexural toughness indexes to characterize the load-deflection curve has been shown. However, it is still relatively difficult to use a set of indexes in design. We need a simpler method of accounting for material brittleness in our design procedure.

Fig. 5 illustrates the theoretical correlation between increasing $f_f/f_t$ ratios and decreasing material brittleness. Comparing Fig. 6 and 7 shows correlation between increasing $f_f/f_t$ ratios and decreases in the initial descending slope of the softening curve for the materials used in this experimental program. Experimental results presented by Petersson[3] for various plain concrete qualities showed the $f_f/f_t$ ratio as an increasing function of the material characteristic length. $f_f/f_t$ increased from 1.73 to 2.29 when $l_{ch}$ increased from 87 to 500 mm (3.4 to 19.7 in.). Neville[18] presented test results for plain concrete showing the $f_f/f_t$ ratio decreasing from 1.78 to 1.57 when concrete compressive strength increases from 20 to 65 MPa (2900 to 9425 psi). Thus, the $f_f/f_t$ ratio portrayed the greater brittleness of higher strength concrete. All these results suggest the possibility of using the simple parameter $f_f/f_t$ as a measure of material brittleness. Calculation of this parameter involves only two fast and simple laboratory tests, and it is thus ideally suited for design and quality control purposes.

Comparison of Fig. 7 and 13 shows that, in general, increases in the flexural toughness index $T_{max}$ corre-

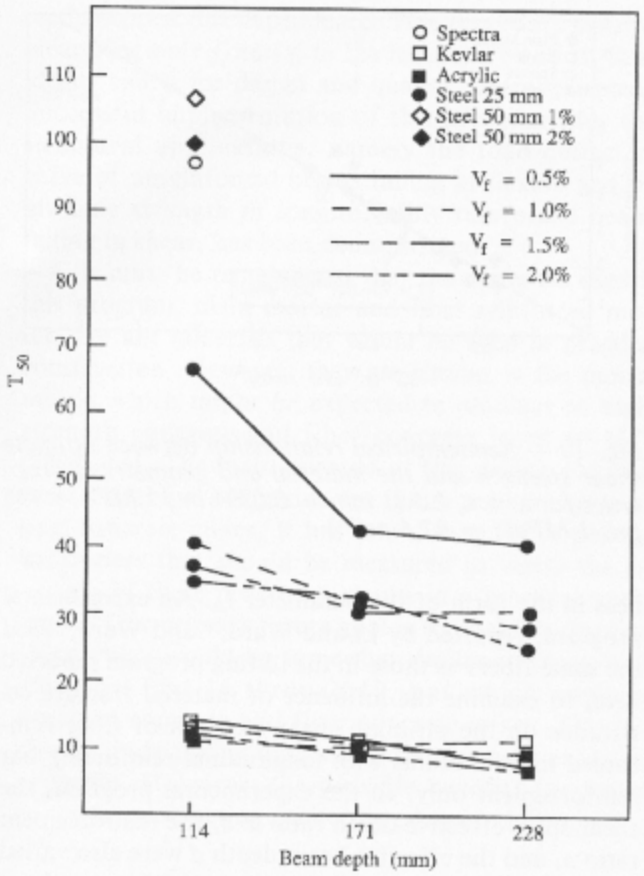


*Fig. 14 — Influence of beam size on flexural toughness index $T_{50}$ (1 mm = 0.0394 in.)*

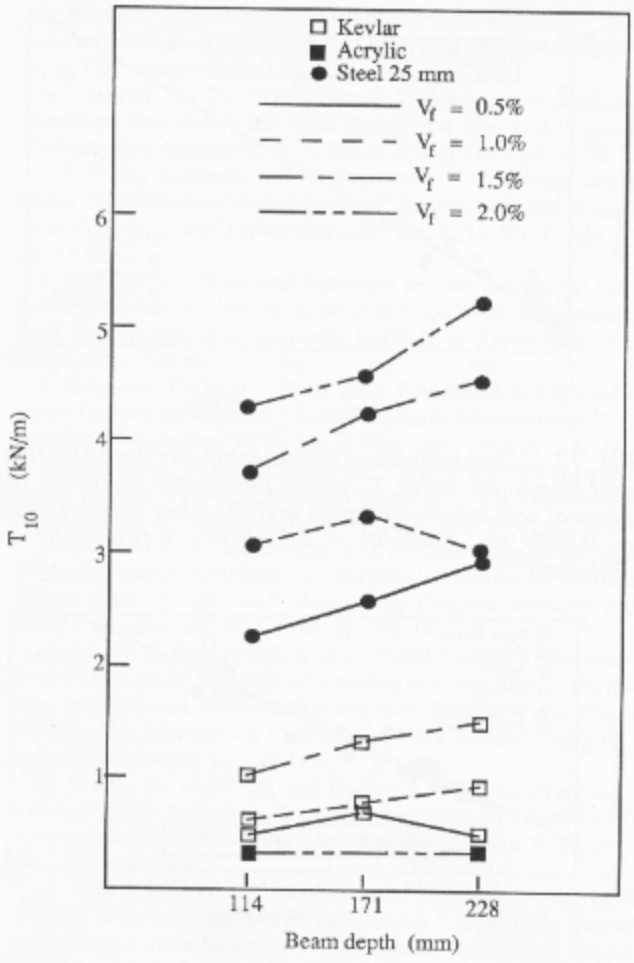


*Fig. 15 — Influence of beam size on flexural toughness index $T_{10}$ (1 mm = 0.0394 in.; 1 kN/m = 5.7 lb/in.)*

spond to increases in the ratio $f_f/f_t$. Fig. 16 illustrates reasonably good straight-line correlation between $(T_{max})^{1/3}$ and $f_f/f_t$ for all materials and beam sizes used in this testing program. The equation for the straight line shown in Fig. 16 is given as

$$(T_{max})^{1/3} = 1.50\, f_f/f_t \qquad (3)$$

A high value of $f_f/f_t$ indicates a material with a relatively flat softening curve, which leads to relatively large inelastic deformation between initial matrix cracking and ultimate flexural strength. This also leads to a high $T_{max}$ value. Also, the size dependence of the parameter $f_f$ accounts for the size dependence of $(T_{max})$.[1/3]

The $T_{10}$ value is influenced both by inelastic energy absorption throughout the beam volume (including energy absorbed by multiple cracking) and also by the fracture energy absorbed across the fracture plane. The $f_f/f_t$ ratio can account for the distributed inelastic energy component. It may be expected that the fracture energy absorbed by the fiber pullout across the fracture zone is related to fiber bond strength and fiber length. A good bond strength gives high stress capacity and a long fiber gives stress transfer capability at relatively large crack opening. Another reasonable assumption is that there is a direct relationship between the flexural strength and the combined bond strengths of all the fibers bridging the critical fracture zone. Thus, flexural

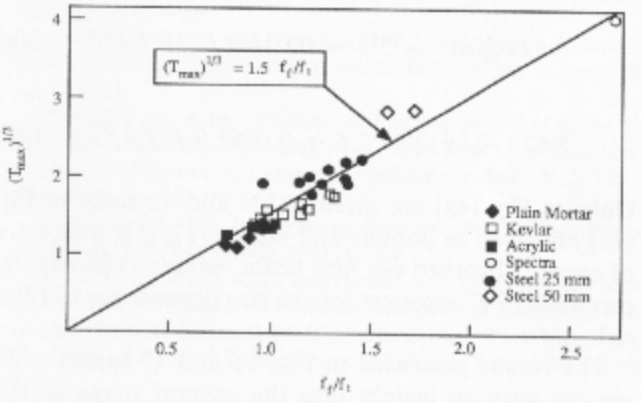


*Fig. 16 — Semiempirical relationship between the flexural toughness index $T_{max}$ and the $f_f/f_t$ ratio (1 mm = 0.0394 in.)*

strength can account for individual fiber bond strength together with the fiber volume fraction. This leads to the product of flexural strength and fiber length $f_f l_f$ as a means of ranking materials according to the fracture energy (note that the units are similar). These arguments lead to the development of Fig. 17, which shows reasonable straight line correlation between the parameter $(f_f/f_t)\, f_f l_f$ and $(T_{10}/d)^{1/3}$, for all materials and beam sizes. The formula for the straight line shown in Fig. 17 is given as

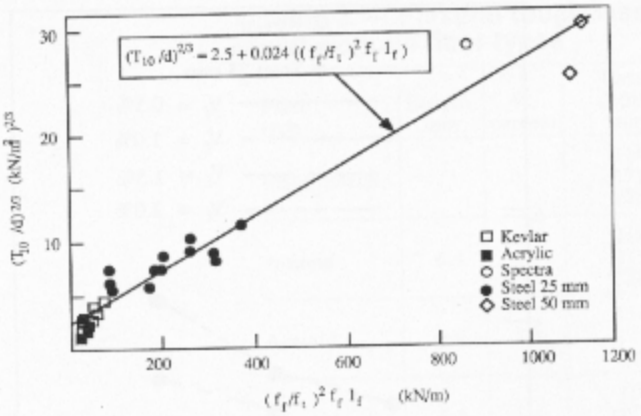


*Fig. 17 — Semiempirical relationship between the flexural toughness index $T_{10}$ and a parameter involving the flexural and tensile strengths and the fiber length [1 mm = 0.0394 in.; 1 kN/m = 5.7 lb/in.; 1 (kN/m$^2$)$^{2/3}$ = .276 (psi)$^{2/3}$]*

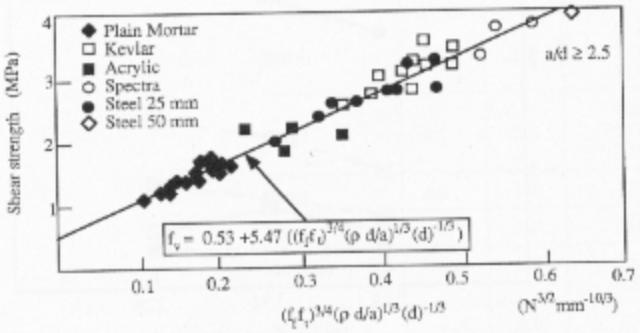


*Fig. 18 — Semiempirical relationship between ultimate shear strength and the material and geometrical properties for a/d ≥ 2.5 (1 mm = 0.0394 in.; 1 MPa = 145 psi; 1N$^{3/2}$ mm$^{-10/3}$ = 5133.6 lb$^{3/2}$in.$^{-10/3}$)*

$$(T_{10}/d)^{1/3} = 2.5 + 0.024\,[(f_f/f_t)^2 f_f l_f] \quad (4a)$$

$$3.62\,(T_{10}/d)^{1/3} = 2.5 + 0.0042\,[(f_f/f_t)^2 f_f l_f] \quad (4b)$$

Units in Eq. (4a) are given in kN and m; units in Eq. (4b) are given in pounds and inches. $T_{10}/d$ is indicative of energy absorbed per unit beam volume. The size dependence of $f_f^2$ accounts for the size dependence of $(T_{10}/d)^{1/3}$.

The results presented in Fig. 16 and 17 suggest that we can gain an insight into the general shape of the flexural load-deflection curve by simply measuring the flexural and tensile strengths. It must be remembered that the measured splitting tensile strength depends on the cylinder size. It should not be unreasonable to suggest that the same standard cylinder size 152.5 x 305 mm (6 x 12 in.), as used for the compression test, be adopted as standard.

## PREDICTING ULTIMATE SHEAR STRENGTH

Gustafsson[4] showed the ratio $f_v/f_t$ as an increasing function of the parameter $l_{ch}/d$, using the fictitious crack model and finite element analysis. This suggests that the structural strength parameter $f_v$ depends on both the material strength $f_t$ and the material brittleness in the form of the parameter $l_{ch}$. An experimental program, reported by Li and Ward,[19] and Ward,[8] used the same fibers as those in the testing program reported here, to examine the influence of material fracture resistance on the ultimate shear strength of fiber reinforced mortar beams with longitudinal reinforcing bar reinforcement only. In the experimental program, the shear span/effective depth ratio $a/d$, the reinforcement ratio $\rho$, and the effective beam depth $d$ were also varied to obtain the dependence of ultimate shear strength on these parameters as well. The results of the experimental program are summarized in Fig. 18 and 19. These results suggest that ultimate shear strength can be predicted by measuring only the flexural and tensile strengths and using a combination of these parameters to quantify the effect of fracture resistance on structural strength.

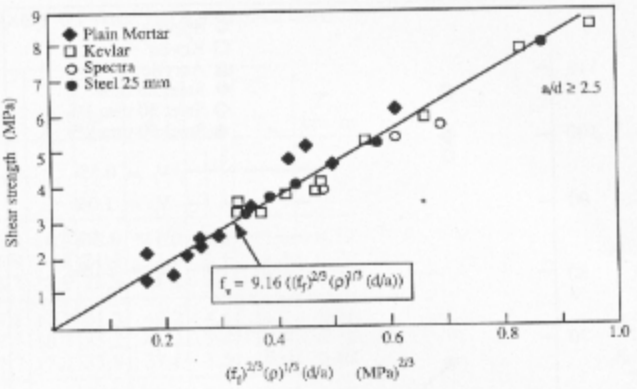


*Fig. 19 — Semiempirical relationship between ultimate shear strength and the material and geometrical properties for a/d ≤ 2.5 (1 mm = 0.0394 in.; 1 MPa = 145 psi; 1 MPa$^{2/3}$ = 27.6 psi$^{2/3}$)*

## CONCLUSIONS

1. The trend of decreasing flexural strength with beam size increases is found to be similar for plain mortar and for mortar reinforced with various steel and synthetic fibers. On average, the flexural strength decreases in proportion to $d^{-0.13}$, for similar beam geometry. The total energy absorbed per unit beam volume decreases as beam size increases, for similar beam geometry.

2. The ratio between the initial downward slope of the tension-softening curve and the slope of the stress-strain curve $l/l_{ch}'$ is a good measure of material brittleness. However, the tension-softening curve is, in general, too difficult and time-consuming to measure for practical implementation in routine design and quality control. Using a direct correlation between the effective material characteristic length $l_{ch}'$ and the $f_f/f_t$ ratio, this ratio is suggested as a simple and practical measure of material brittleness, a low value signifying a brittle material.

3. By realizing the dependence of structural behavior on material fracture resistance, and also the ability of the parameters $f_f$ and $f_t$ to characterize this dependence, it is possible to develop simple formulas that di-

rectly express this dependence. This procedure involves measuring only $f_f$ and $f_t$ in the laboratory and is, thus, ideally suited for design and quality control purposes. Successful implementation of this procedure for two structural applications, namely the load-deflection curve of unreinforced beams failing in flexure and the ultimate strength of longitudinally reinforced beams failing in shear, has been demonstrated.

4. It must be remembered that the materials used in this program, plain mortar and fiber reinforced mortar, are not materials that would be used in practical construction. However, they are similar to the mortar matrix which might be expected in medium to high-strength concrete and fiber concrete [over 40 MPa (5800 psi)]. The main purpose of this testing program was to establish a direction for future research on practical concrete mixes. It has established the important parameters that should be measured to verify the extension of these promising results in a practical application. Our primary future goal is to establish relationships which would be somewhat similar to those illustrated in Fig. 16 through 19, but which apply to practical concrete and fiber concrete mixes. This is a sizable undertaking and would require a large testing program. However, the possible benefits for future concrete construction cannot be overstated.

## ACKNOWLEDGMENTS

The authors gratefully acknowledge the support of the National Science Foundation. They would also like to thank S. Backer, Y. Wang, and E. Green for many helpful discussions during the course of this work.

## REFERENCES

1. Hillerborg, A., "Analysis of One Single Crack," *Fracture Mechanics of Concrete,* Elsevier Science Publishers, Amsterdam, 1983, pp. 223-250.

2. Hillerborg, A., "Fracture Mechanics and the Concrete Codes," *Fracture Mechanics: Application to Concrete,* SP-118, American Concrete Institute, Detroit, 1989, pp. 157-169.

3. Petersson, Per-Erik, "Crack Growth and Development of Fracture Zones in Plain Concrete and Similar Materials," *Report* No. TVBM-1006, Division of Building Materials, Lund Institute of Technology, 1981, 174 pp.

4. Gustafsson, Per Johan, "Fracture Mechanics Studies on Non-Yielding Materials like Concrete," *Report* No. TVBM-1007, Division of Building Materials, Lund Institute of Techonology, 1985, 422 pp.

5. Henager, C. H., "Toughness Index of Fibre Concrete," *Testing and Test Methods of Fibre Cement Composites* (RILEM Symposium 1978), Construction Press Ltd., Lancaster, pp. 79-86.

6. Johnston, C. D., "Definition and Measurement of Flexural Toughness Parameters for Fiber Reinforced Concrete," *Cement, Concrete, and Aggregates,* V. 4, No. 2, Winter 1982, pp. 53-60.

7. Wang, Youjiang, and Backer, Stanley, "Toughness Determination for Fibre Reinforced Concrete," *International Journal of Cement Composites and Lightweight Concrete,* V. 11, No. 1, Feb. 1989, pp. 11-19.

8. Ward, R. J., "Structural Behaviour of Fiber Reinforced Mortar Related to Material Fracture Resistance," SM thesis, Department of Civil Engineering, Massachusetts Institute of Technology, Cambridge, June 1989.

9. Johnston, Colin D., "Steel Fiber Reinforced and Plain Concrete: Factors Influencing Flexural Strength Measurement," ACI JOURNAL, *Proceedings* V. 79, No. 2, Mar.-Apr. 1982, pp. 131-138.

10. Akihama, Shigeyuki; Suenaga, Tatsuo; and Nakagawa, Hiroaki, "Carbon Fiber Reinforced Concrete," *Concrete International; Design & Construction,* V. 10, No. 1, Jan. 1988, pp. 40-47.

11. Torrent, R. J., and Brooks, J. J., "Application of the Highly Stressed Volume Approach to Correlated Results from Different Tensile Tests of Concrete," *Magazine of Concrete Research* (London), V. 37, No. 132, Sept. 1985, pp. 175-184.

12. Li, V. C., and Ward, R. J., "Novel Testing Technique for Post-Peak Tensile Behavior of Cementitious Materials," *Proceedings,* International Workshop on Fracture Toughness and Fracture Energy—Test Methods for Concrete and Rock (Sendai, 1988), A. A. Balkema Publishers, pp. 183-196.

13. Wang, Y.; Li, V. C.; and Backer, S., "Tensile Properties of Synthetic Fiber Reinforced Mortar," *International Journal of Cement Composites and Lightweight Concrete* (Harlow), V. 12, No. 1, Feb. 1990, pp. 29-42.

14. Hillerborg, Arne, "Determination and Significance of the Fracture Toughness of Steel Fibre Concrete," *Steel Fiber Concrete* (U.S.-Sweden Joint Seminar, 1985), Swedish Cement and Concrete Institute, Stockholm/Elsevier Applied Science Publishers, London, 1986, pp. 257-271.

15. ACI Committee 544, "State-of-the-Art Report on Fiber Reinforced Concrete," (ACI 544.1R-73), American Concrete Institute, Detroit, 1973, 16 pp.

16. Hibbert, A. P., and Hannant, D. J., "Toughness of Fiber Cement Composites," *Composites* (Guildford), V. 13, No. 2, Apr. 1982, pp. 105-111.

17. Hillerborg, Arne, "Analysis of Fracture by Means of the Fictitious Crack Model, Particularly for Fiber Reinforced Concrete," *International Journal of Cement Composites* (Harlow), V. 2, No. 4, Nov. 1980, pp. 177-184.

18. Neville, A. M., *Properties of Concrete,* 3rd Edition, Pitman Publishers, Inc., Marshfield, 1981, p. 304.

19. Li, V. C.; Ward, R. J.; and Hanza, A., "Effect of Fiber Modified Fracture Properties on the Shear Resistance of Reinforced Mortar and Concrete Beams," RILEM International Workshop on Applications of Fracture Mechanics to Reinforced Concrete, Torino, 1990.